Morphological, immunophenotypic and neuroradiological characteristics of primitive B-large cell diffuse lymphoma of the central nervous system: A retrospective cohort analysis

IDA RIZZUTO[1*], CRISTINA PIZZIMENTI[1*], VINCENZO FIORENTINO[1], SARAH CAROLINE SCARCELLA[2], MAURIZIO MARTINI[1], FRANCESCA GRANATA[2], ANTONINO GERMANÒ[2], ANTONIO IENI[1] and GIOVANNI TUCCARI[1]

[1]Department of Human Pathology in Adult and Developmental Age, 'Gaetano Barresi' Section of Pathology, University of Messina, I-98125 Messina, Italy; [2]Department of Biomedical, Dental, Morphological, and Functional Imaging Sciences, University of Messina, I-98125 Messina, Italy

Received April 9, 2025; Accepted June 16, 2025

DOI: 10.3892/ol.2025.15179

Abstract. Primitive diffuse large B-cell lymphoma (PCNSL-DLBCL) accounts for 2-3% of all central nervous system (CNS) tumors, predominantly affecting supratentorial sites in adult patients. In the present study, the immunohistochemical (IHC) profile was analyzed in a cohort of 23 cases of CNS DLBCL to determine whether B-cell markers [CD20, CD79a and paired box 5 (PAX5)], BCL2, CD10, BCL6, MUM1 and c-Myc, as well as the Ki67 labeling index, were associated with the clinicopathological (age, sex and location) and neuroradiological (T1, T2, post-contrast and diffusion-weighted imaging) parameters of the patients. The Hans algorithm was applied to subtype DLBCLs into germinal center B-cell (GCB) and non-germinal center B-cell (non-GCB). Univariate statistical analysis was performed using Fisher's exact test to identify statistically significant associations between clinicopathological, IHC and radiological variables. Multivariate analysis was then conducted to assess the independent effects of these variables on overall survival (OS). The most frequent site of PCNSL-DLBCL was confirmed in supratentorial areas, with invasion of midline structures; 7 cases presented with a single lesion, while 11 exhibited multifocal disease. All cases exhibited positive expression of CD20, PAX5 and CD79a; 21 cases exhibited positive expression of BCL2. The mean Ki67 labeling index was 80%. A total of 17 cases were classified as non-GCB and 6 as GCB. A statistically significant association was documented between the site of the disease and the number of lesions (P=0.04), the site of disease and subtype (P=0.03), and the IHC subtype and mean enhancement value (P=0.008). The present study demonstrated that DLBCL with a non-GCB immunohistochemical profile was predominantly observed in patients with unfavorable prognostic factors, such as age >60 years, a high Ki67 labeling index and shorter OS. Statistically significant associations were found between disease location and the number of lesions, disease location and IHC subtype, and between IHC subtype and the mean enhancement value, which may serve as predictors for the IHC subtype. Multivariate analysis and Kaplan-Meier curves revealed that the IHC subtype and enhancement value were independent prognostic factors, with the GCB profile and higher enhancement values being associated with longer OS times and improved prognosis (P=0.0158). In conclusion, the identified associations suggested that the IHC subtype and apparent diffusion coefficient neuroimaging parameters were useful validated prognostic indicators.

Correspondence to: Professor Giovanni Tuccari, Department of Human Pathology in Adult and Developmental Age, 'Gaetano Barresi' Section of Pathology, University of Messina, Via Consolare Valeria 1, I-98125 Messina, Italy
E-mail: tuccari@unime.it

*Contributed equally

Key words: B-large cell diffuse lymphoma, extranodal non-Hodgkin lymphoma, central nervous system, immunohistochemistry, prognosis

Introduction

Primary Central Nervous System Lymphoma is an uncommon and highly aggressive form of primitive extranodal Non-Hodgkin Lymphoma (NHL), accounting for 3% of all brain tumors. Its incidence has increased in recent decades, accounting for 0.47/100,000 people, with a male-to-female ratio of 1.2:1.7, with the highest rates observed in patients over 60 (1). The main known risk factor for PCNSL is immunodeficiency, whether primary or acquired, due to HIV infection or organ transplants (2-4). The most frequent histological subtype of PCNSL is Diffuse Large B-cell lymphoma, which comprises 95% of cases (5). PCNSL has been reported to occur in brain parenchyma, spinal cord, meninges, and ocular tissues, although the most common site is supratentorial (5). Distinctive topographic features include the involvement of the midline structures, such as the corpus callosum and fornix, and locations adjacent to cerebrospinal

fluid spaces, in contact with the ependymal surface (5). Infratentorial locations in the brainstem and cerebellum or involvement of cranial nerves are uncommon (5). This site variability may explain the pleomorphic symptoms, with headache and seizures being the most common (6). Cerebral stereotaxic biopsy is considered the gold standard for diagnosis, although it should be performed without prior corticosteroid treatment, which can promote lymphocellular necrosis and compromise accurate diagnosis (5-7). The usual morphological features include large necrotic areas with evidence of neoplastic lymphocytes invading the surrounding parenchyma. This proliferation consists of pleomorphic and atypical B lymphoid cells with large round nuclei, prominent nucleoli, and many mitoses (8). Additionally, mixed reactive inflammatory cells, including T lymphocytes, are found among B-cells (9). The angiocentric growth pattern, with vessels surrounded by neoplastic lymphocytes, can be a significant morphological feature (8,10). Using Hans' algorithm, two main immunohistochemical subtypes can be identified: Germinal and Non-Germinal Centre B-cell (11). Specifically, the GCB subtype exhibits immunoreactivity for CD10 and BCL-6, while Non-GCB can be further subdivided into Activated B-Cell (ABC) with immunoreactivity for MUM1 and an unclassified subtype (11). The GCB subtype has a reportedly better clinical outcome compared to Non-GCB (11). The neuroradiological key points for diagnosing PCNSL include evidence of solid, sometimes multiple, supratentorial masses with low Apparent Diffusion Coefficient (ADC) on diffusion-weighted Magnetic Resonance Imaging (MRI) sequences and homogeneous enhancement after Gadolinium-diethylenetriamine pentaacetic acid (DTPA) administration. In immunocompromised patients, the MRI pattern is less specific, often revealing intralesional hemorrhage or necrosis with ring-like enhancement after Gadolinium administration (12). This retrospective multidisciplinary study aims to analyze a cohort of 23 patients affected by PCNSL-DLBCL, comparing their clinical, pathological, and neuroradiological features and evaluating the potential effects of these variables on OS.

Materials and methods

Patients and tumor specimens. Clinical and pathological data from 23 patients diagnosed with PCNSL-DLBCL between January 2012 and November 2024 were obtained through neurosurgical procedures and collected from the Department of Human Pathology of Adult and Developmental Age, Section of Pathological Anatomy, University of Messina, A.O.U. Gaetano Martino (Messina, Italy). The analysis was performed according to Good Clinical Practice guidelines and the Declaration of Helsinki (1975, revised in 2013). Before the surgical procedures, all patients provided written, anonymized, and informed consent. Pathology reports and medical records were thoroughly reviewed. Patients' initials and other personal identifiers were removed from all images. The Institutional Review Board of the University Hospital of Messina (Messina, Italy) approved this study vide protocol no. 47/19 of May 2, 2019. Data collected included age at diagnosis, gender, and site of disease, classified as supratentorial or infratentorial. MRI images of the aforementioned patients were collected from the Department of Biomedical, Dental, Morphological, and Functional Imaging Sciences, Section of Neuroradiology, University of Messina, A.O.U. Gaetano Martino (Messina, Italy), including T1 and T2 weighted images, Late Gadolinium Enhancement (LGE) imaging, and Diffusion-weighted Imaging (DWI), considering the ADC as a surrogate for neoplastic cellularity and the mean Ki-67 value of enhancement as an expression of blood-brain barrier (BBB) damage. After surgical procedures, all patients underwent radio-chemotherapy with four cycles of methotrexate, cytarabine, rituximab, and prednisolone; additionally, complementary whole-brain radiotherapy (30-36 Gy) was performed.

Immunohistochemical analysis. All tumor specimens were fixed in 10% neutral-buffered-formalin at room temperature for 24 h and paraffin-embedded. Five-micron-thick sections were obtained from corresponding tissue blocks for hematoxylin and eosin (H&E) routine staining. Parallel sections from the same tissue blocks were cut for immunohistochemical procedures; slides were deparaffinized in xylene, dehydrated, and treated with 3% hydrogen peroxide for 10 min to block endogenous peroxidase; they were then washed in deionized water thrice (10 min each time). Sections were incubated with normal sheep serum to prevent nonspecific adherence of serum proteins for 30 min at room temperature. Thereafter, sections were again washed with deionized water and incubated for 30 min at 37˚C with the working dilution suggested by the ROCHE manufacturer for each commercially obtained monoclonal antibody. The following monoclonal antibodies against CD20 (L26), PAX5 (SP34), CD79a (SP18), GFAP (EP672Y), BCL-2 (124), Ki-67 (MIB 1), CD10 (SP67), BCL-6 (GI191E/A8), and MUM1 (EP190) were used. Subsequently, sections were washed with phosphate-buffered saline solution (PBS) at pH 7.2-7.4 and incubated with corresponding secondary antibodies (1:300; Abcam, code no. ab7064) for 20 min at room temperature, incubated with horseradish peroxidase-labeled secondary antibody for 30 min and developed with diaminobenzidine tetrahydrochloride, counterstained with hematoxylin using the ULTRA Staining system (Ventana Medical Systems). Negative controls were obtained by omitting the specific antisera and substituting PBS for the primary antibody. The immunohistochemical staining for each sample was independently scored by two pathologists, who were blinded to patient outcomes and clinical findings, using a Zeiss Axioskop microscope (Carl Zeiss Microscopy GmbH) at 40x objective magnification. Staining for CD10, BCL-6, and MUM-1 was considered positive when >30% of cells were positively stained; staining for BCL-2 was considered positive when >50% of cells were positively stained. Ki-67 expression was evaluated as high when the percentage of positive neoplastic cells was >50%, counting at least 1,000 cells.

Immunophenotype classification. Two main subtypes of PCNSL-DLBCL were identified through the combined expression of CD10, BCL-6, and MUM-1. All CD10+ tumor phenotypes were classified as the GCB subgroup. Samples with CD10-BCL-6+ MUM-1+ and CD10-BCL-6-MUM-1+ profiles were considered Non-GCB subtypes.

MRI protocol. All MRI examinations were performed in the clinical routine using a 1.5 Tesla MRI scanner (Ingenia

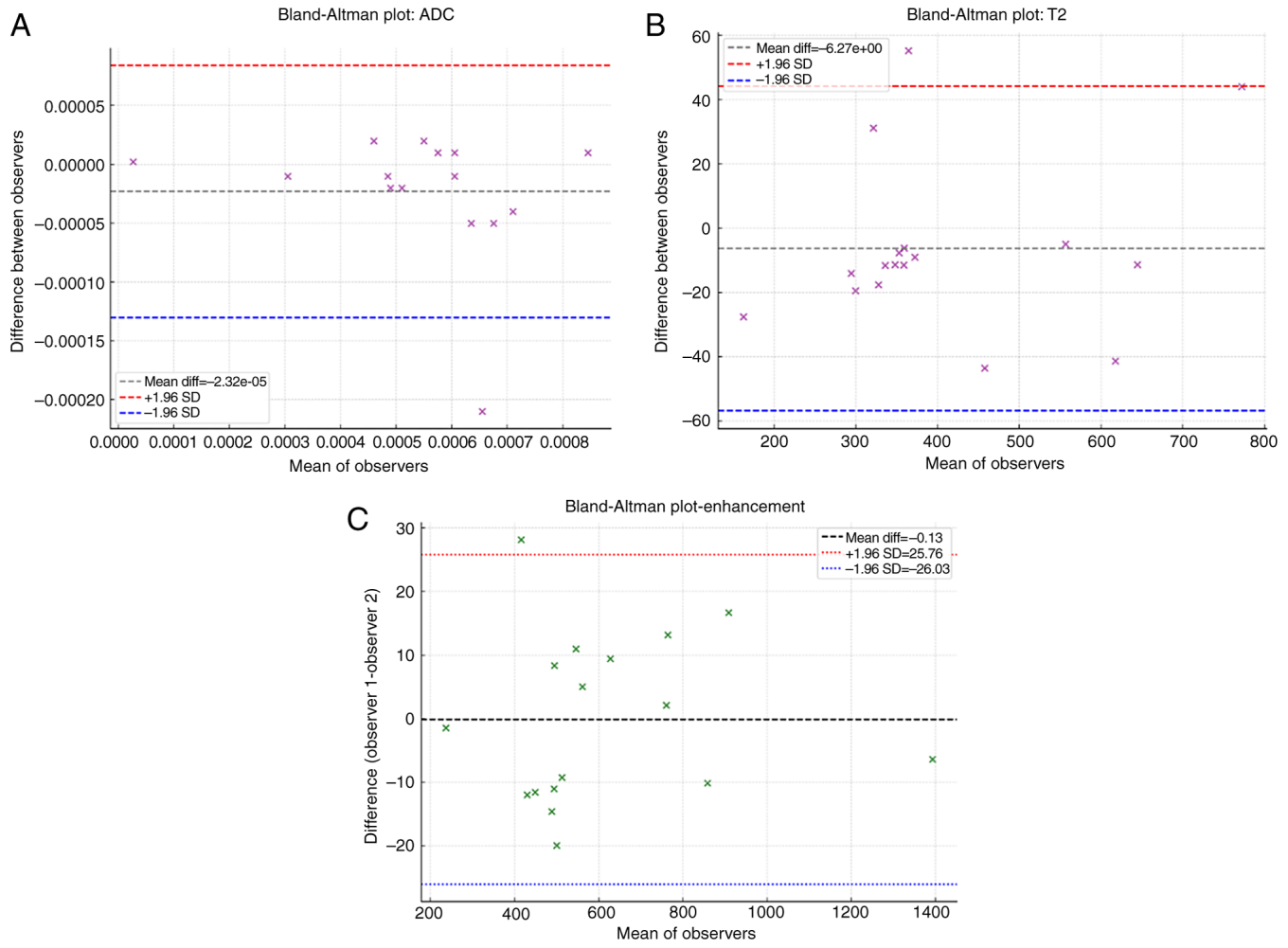

Figure 1. Bland-Altman plots to assess agreement between the two observers. Good inter-observer agreement was demonstrated for (A) ADC, (B) T2 signal and (C) enhancement. ADC, apparent diffusion coefficient; difference.

Philips Healthcare, Best, The Netherlands). The MRI protocol included: axial DWI single-shot spin-echo (SE) echo planar sequence (repetition time (TR)/echo time (TE): 3000/85 ms, flip angle (FA): 90˚, SL: 71.6 mm, slice thickness (ST): 5 mm, field of view (FOV): 230 mm). Diffusion-sensitizing gradients were applied sequentially in the x, y, and z directions with b factors of 0 and 1,000 s/mm^2. ADCs were automatically calculated by the MR scanner and displayed as corresponding ADC maps: axial SE T1-weighted sequence (TR: 633 ms, TE: 15 ms, FA: 69˚, SL: 71 mm, ST: 5.50 mm); axial fast SE (FSE) T2-weighted sequence (TR: 4848 ms, TE: 100 ms, FA: 90˚, SL: 71.60 mm, ST: 5 mm); 3D fluid-attenuated inversion recovery (FLAIR-3D) sequence (TR: 5200 ms, TE: 305 ms, FA: 90˚, SL: 21.44 mm); postcontrast 3D T1-weighted gradient-echo (GE) sequence (TR/TE: 25/4.58 ms, FA: 30˚, 1-mm section thickness, and 230 mm FOV). A standard dose (0.1 mmol/kg body weight) of gadoteric acid (Gd-DOTA, Dotarem; Laboratoire Guerbet, Aulnay-sous-Bois, France) was injected intravenously.

Image analysis. All images were available in digital format. Image analysis was performed on a Philips Portal Viewer. T2 and ADC maps were co-registered with the post-contrast T1-weighted 3D-gradient echo sequence. Image analysis was conducted by two independent neuroradiologists, who drew a circular Region-of-Interest (ROI) within the tumor, avoiding regions suspected of intralesional hemorrhage or necrosis. Three sets of data were collected, including ADC, T2 signal, and enhancement evaluation. A Bland-Altman plot was used to assess agreement between the two observers (Fig. 1). Good inter-observer agreement was demonstrated for all MRI parameters: ADC (Fig. 1A), T2 signal (Fig. 1B), and enhancement (Fig. 1C).

Statistical analysis. The association between the immunohistochemical profile of tumors, clinicopathological (age, sex, and site of disease), and neuroradiological features was subjected to univariate analysis with Fisher's exact test. Multivariate analysis was performed using the Cox regression model to study the independent effects of variables on OS, defined as the time from diagnosis to death. Kaplan-Meier survival curves were generated. All statistical evaluations were performed using MedCalc version 10.2.0.0 (MedCalc Software). Results were considered statistically significant when $P<0.05$.

Results

Histology and immunohistochemical results. All cases exhibited typical morphological features of PCNSL-DLBCL in hematoxylin

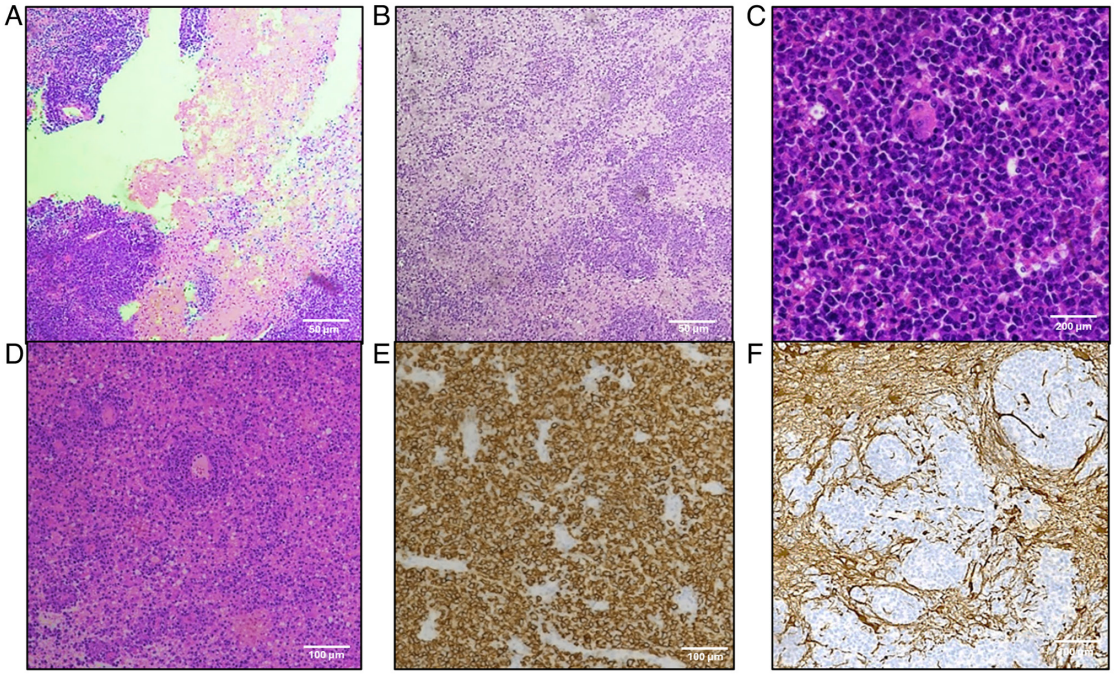

Figure 2. Primitive diffuse large B-cell lymphoma: Histologic and immunohistochemical features. (A) Large areas of geographical necrosis (hematoxylin and eosin staining; magnification, x100; scale bar, 50 μm). (B) Clusters of tumor cells invading brain parenchyma (hematoxylin and eosin staining; magnification, x100; scale bar, 50 μm). (C) Atypical B cells with big, round, vesicular nuclei and numerous mitoses (hematoxylin and eosin staining; magnification, x400; scale bar, 200 μm). (D) Angiocentric pattern of growth (hematoxylin and eosin staining; magnification, x100; scale bar, 100 μm). (E) Diffuse cell membrane CD20-positivity (Mayer's hemalum nuclear counterstain; magnification, x200; scale bar, 100 μm). (F) $GFAP^-$ tumor cells invading $GFAP^+$ brain parenchyma (Mayer's hemalum nuclear counterstain; magnification, x200; scale bar, 100 μm). GFAP, glial fibrillary acidic protein.

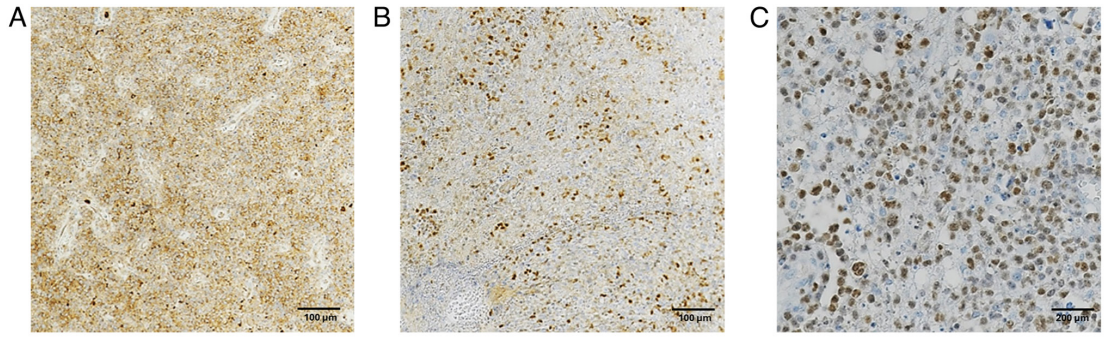

Figure 3. Primitive diffuse large B-cell lymphoma: GCB and non-GCB phenotype. (A) Cell membrane CD20-positivity in the GCB subtype (Mayer's hemalum nuclear counterstain; magnification, x200; scale bar, 100 μm). (B) Nuclear BCL-6-positivity in the GCB subtype (Mayer's hemalum nuclear counterstain; magnification, x200; scale bar, 100 μm). (C) Nuclear MUM-1-positivity in the non-GCB subtype (Mayer's hemalum nuclear counterstain; magnification, x400; scale bar, 200 μm). GCB, germinal center B-cell.

and eosin sections (Fig. 2). B-cell markers (CD20, PAX5, and CD79a) demonstrated cell membrane staining in all specimens. Twenty-one out of 23 cases indicated nuclear BCL-2 immunoreactivity. Lymphoid clusters were GFAP negative, with infiltration of GFAP-positive adjacent nervous tissue. In 17 out of 23 specimens, nuclear immunoreactivity for c-Myc was documented in >40% of tumor cells. According to Hans' algorithm, 6 samples (26%) were classified as GC: 4 (67%) were CD10+ BCL-6+ MUM-1+; 2 (33%) were CD10+ BCL-6+ MUM-1-. Seventeen tumors (74%) were classified as Non-GCB: 16 (94%) were CD10-BCL-6+ MUM-1+; 1 (6%) was MUM-1+ only (Fig. 3).

Clinicopathological and neuroradiological features. Of the total of 23 patients, 20 (87%) were ≥60, and 3 (13%) were <60, with a median age of 66 and a mean age of 65.7; 8 patients (35%) were male and 15 (65%) female. Supratentorial disease was documented in 18 cases (78%), and infratentorial disease in 5 cases (22%) (Table I). Regarding neuroradiological features, MRI images showed homogeneous enhancement in 21 out of 23 cases and ring enhancement in 2 out of 23 patients, which can be considered an expression of central tumor necrosis. Fourteen out of 18 supratentorial cases revealed invasion of the corpus callosum and other median line structures, while infratentorial cases did not exhibit this feature. Multifocal disease was indicated in 14 out of 23 cases and unifocal disease in 9 out of 23 cases (Fig. 4). The mean ADC value was $0.53x10^{-3}$ mm^2/s, with a standard deviation of $0.18x10^{-3}$ mm^2/s. The mean enhancement

Table I. Clinical and pathological characteristics of patients with primitive diffuse large B-cell lymphoma.

Characteristics	All patients (n=23)	GCB	Non-GCB
Mean age, years (range)	65.7 (44-77)	65.2 (57-75)	65.9 (44-77)
Median age, years	66	65	66
Age, n (%)			
≥60 years	20 (87)	4 (20)	16 (80)
<60 years	3 (13)	2 (67)	1 (33)
Sex, n (%)			
Male	8 (35)	2 (25)	6 (75)
Female	15 (65)	4 (27)	11 (73)
Site of disease, n (%)			
Supratentorial	18 (78)	3 (17)	15 (83)
Infratentorial	5 (22)	3 (60)	2 (40)
Number of lesions, n (%)			
1	9 (39)	1 (11)	8 (89)
≥2	14 (61)	6 (43)	8 (57)

GCB, germinal center B-cell; non-GCB, non-germinal center B-cell.

Table II. Univariate analysis concerning site and number of lesions in patients with primitive diffuse large B-cell lymphoma.

		Number of lesions		
Site of disease	No.	Multifocal, n (n=14)	Unifocal, n (n=9)	P-value
Supratentorial	18	13	5	0.04
Infratentorial	5	1	4	

Table III. Univariate analysis concerning site and histological subtype in patients with primitive diffuse large B-cell lymphoma.

		Subtype		
Site of disease	No.	GCB, n (n=6)	Non-GCB, n (n=17)	P-value
Supratentorial	18	3	15	0.03
Infratentorial	5	3	2	

GCB, germinal center B-cell; non-GCB, non-germinal center B-cell.

value was 613.75, with a standard deviation of 264.66. Two subgroups were identified based on age: those ≥60 included 4 GCB cases (20%) and 16 Non-GCB cases (80%), with a mean Ki-67 value >80%; the second subgroup included 2 GCB cases and 1 Non-GCB case, with a mean Ki-67 value of 57%. The mean Ki-67 value was 82.5% in male patients and 71% in female patients.

Statistical analysis. Univariate analysis revealed significant statistical associations between the following variables: site of disease and number of lesions (P=0.04), site of disease and immunohistochemical (IHC) subtype (P=0.03), gender and ADC (P=0.02), and IHC subtype and mean value of enhancement (P=0.008) (Tables II-V). In multivariate analysis, IHC subtype (P=0.0158) (Fig. 5) and mean value of enhancement (P=0.0391) (Fig. 6) emerged as independent variables; comparing survival curves for GCB vs. Non-GCB and low vs. high enhancement revealed significant differences in OS. Additionally, a trend toward statistical significance was observed for c-Myc (P=0.0648).

Discussion

PCNSL is reportedly an uncommon extranodal lymphoma with a poor prognosis (1,2). In the present study, we analyzed

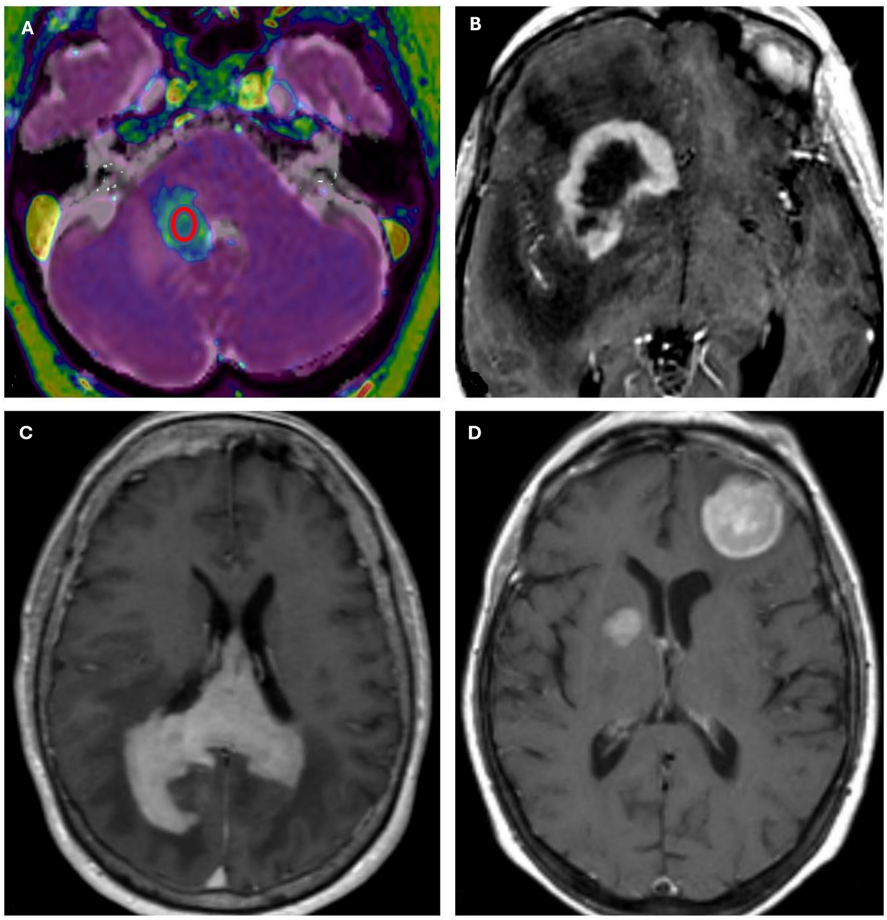

Figure 4. MRI features of primitive diffuse large B-cell lymphoma. (A) T1 magnetization prepared rapid gradient echo post-gadolinium administration/ADC co-registration. A region-of-interest (red circle) was drawn in the ADC map at the center of a right cerebellar lesion. (B) Ring enhancement indicative of central necrosis (post-contrast T1-weighted MRI). (C) Corpus callosum infiltration (post-contrast T1-weighted MRI). (D) Multifocal disease (post-contrast T1-weighted MRI). ADC, apparent diffusion coefficient.

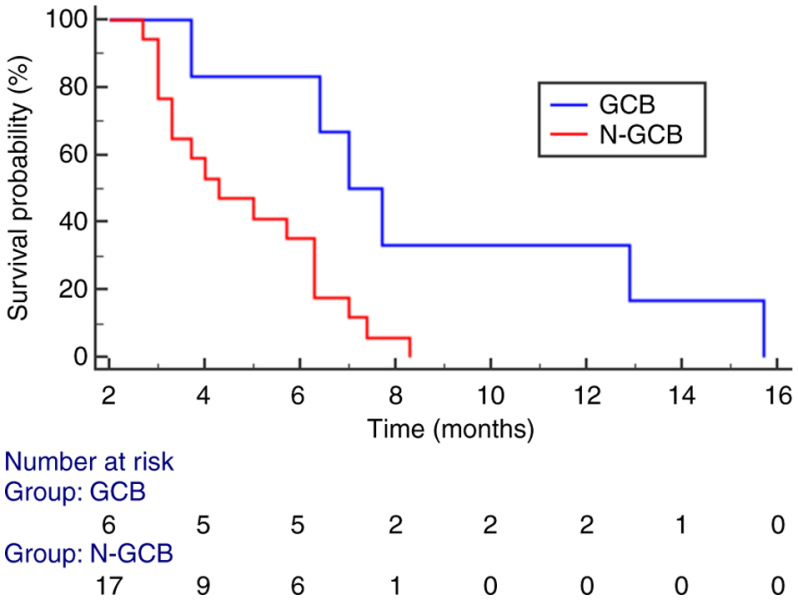

Figure 5. Comparison of the overall survival time between the GCB and N-GCB subtypes. GCB, germinal center B-cell; N-GCB, non-germinal center B-cell.

a cohort of PCNSL-DLBCL patients, documenting a higher incidence in those aged ≥60, consistent with existing literature (5). We also confirmed the highest occurrence of the disease in supratentorial sites, as found elsewhere too (13,14).

Table IV. Univariate analysis concerning sex and ADC in patients with primitive diffuse large B-cell lymphoma.

		ADC		
Sex	No.	>0.53x10^{-3} mm^2/sec, n (n=12)	<0.53x10^{-3} mm^2/sec, n (n=11)	P-value
Male	8	7	1	0.02
Female	15	5	10	

ADC, apparent diffusion coefficient.

Table V. Univariate analysis concerning histological subtype and MRI enhancement in patients with primitive diffuse large B-cell lymphoma.

		Mean value of enhancement		
IHC subtype	No.	>613.75, n (n=8)	<613.75, n (n=15)	P-value
GCB	6	5	1	0.008
Non-GCB	17	3	14	

GCB, germinal center B-cell; non-GCB, non-germinal center B-cell; IHC, immunohistochemical.

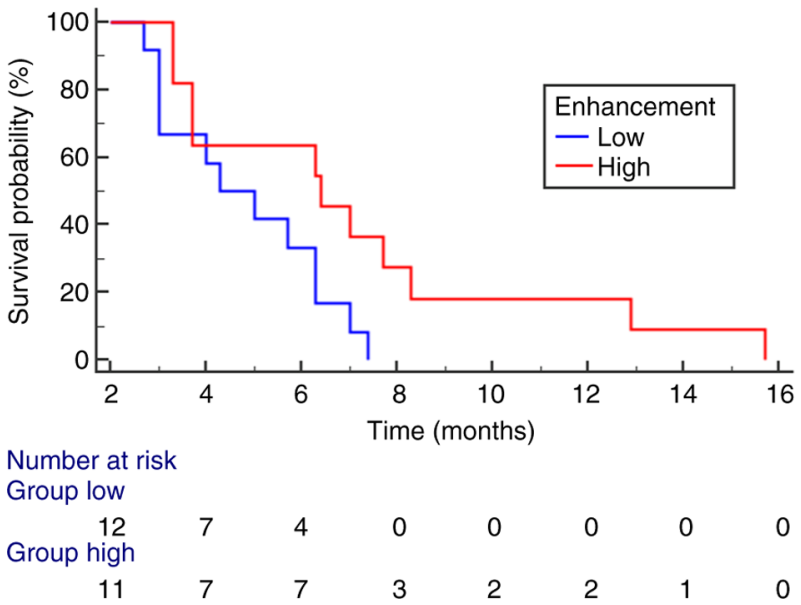

Figure 6. Comparison of overall survival time between low and high enhancement value groups.

Interestingly, our cohort showed a higher number of affected female patients than males (13,15). Notably, concerning the growth fraction in PCNSL-DLBCL, the mean Ki-67 value appeared slightly reduced in the female subgroup (Ki-67=71%) compared to male patients (Ki-67=82.5%). However, a higher mean value (>80%) was observed in patients aged ≥60 compared to those <60 (Ki-67 mean value=57%), highlighting higher proliferation rates in older patients (≥60), supporting the potential prognostic significance of age, as indicated by the IELSG main prognostic clinical score (16-18). Additionally, high Ki-67 expression may predict poor prognosis in PCNSL, as Ki-67 >90% has been associated with shorter OS (15).

Our data regarding the prevalence of specific PCNSL-DLBCL phenotypes revealed more Non-GCB cases, with the majority expressing MUM1. Non-GCB cases represented the majority in our cohort (17/23), while GCB cases were only 6/23, aligning with literature data (13,15). Unfortunately, the Non-GCB subtype is associated with a worse prognosis, as it carries additional unfavorable prognostic factors, such as age ≥60 and mean Ki-67 value >80%; conversely, the GCB subtype is associated with a better prognosis, influenced by younger

age (<60) and reduced Ki-67 value (57%). It is well established that Gadolinium-based contrast agents leak from blood vessels into brain tissue due to increased vascular permeability caused by tumor-induced breakdown of the BBB (19). We therefore hypothesize that the GCB subtype of PCNS-DLBCL may exhibit a greater tendency to induce alterations in the capillary bed at the lesion site, resulting in significant alterations in the BBB and consequently, in a marked degree of contrast enhancement on MRI examination. However, in the neuroradiological evaluation of PCNSL, DWI and ADC maps are essential tools, as they provide crucial information about tumor microstructure. Specifically, DWI sequences measure the movement of water molecules in biological tissues, enabling surrogate assessment of tissue characteristics in both normal and pathological conditions (20). In highly cellular tumors, for instance, the movement of water molecules is restricted; thus, hypercellular tumors such as PCNSL typically exhibit low ADC values (21). Further, PCNSL shows lower ADC values than tumors such as glioblastoma multiforme (GBM), metastases, demyelinating lesions, and infections (21). Although GBM may present solid areas with restricted diffusion, it exhibits variable cellularity and may show areas of necrosis or cysts, resulting in greater water diffusion and higher ADC values. Consequently, ADC values in GBM tend to be less homogeneous and higher than in PCNSL (21). Previous studies have indicated a cut-off ADC value of $0.69x10^{-3}$ mm^2/s (21) that can help distinguish lymphoma from glioblastoma with high sensitivity and specificity. In our case series, all patients had brain lesions with low ADC values (mean ADC value $0.53x10^{-3}$ mm^2/s, with a standard deviation of $0.18x10^{-3}$ mm^2/s), with no significant difference between GCB and Non-GCB groups. Further, we were unable to identify a statistically significant inverse correlation between lesional ADC values and cellular growth fraction measured by Ki-67, confirming findings reported elsewhere (22-24). ADC/cellularity correlation varies across different tumor types: strong in neoplasms such as gliomas, ovarian or lung cancer, moderate in epithelial neoplasms, and weak in lymphomas (25). Therefore, the low ADC values observed in lymphomas may be attributable not solely to tumor hypercellularity but to other histopathological features, such as reduced extracellular matrix, stroma/parenchyma ratio, and/or microvessel density (25). Univariate statistical analysis revealed a significant association between the site of PCNSL-DLBCL and the number of lesions (P=0.04), indicating that supratentorial localization is related to multifocality and infratentorial disease to unifocal sites. Additionally, a relationship between this parameter and the IHC subtype emerged (P=0.03), with the supratentorial disease being linked to the Non-GCB subtype and infratentorial disease with the GCB subtype. Other notable correlations were documented, particularly between the IHC subtype and the degree of contrast enhancement (P=0.008), with the GCB subtype demonstrating significantly increased contrast enhancement than the Non-GCB group. Nevertheless, previous studies have attempted to examine the prognostic role of key immunohistochemical markers such as CD10, BCL-6, MUM-1, and BCL-2, along with clinical parameters (age, gender, and the number of lesions), although discordant results have emerged, possibly due to limited cohorts, differing methods of immunohistochemical analysis, and different treatment (15,26). Multivariate analysis and comparison of Kaplan-Meier survival curves indicated that IHC subtype and contrast enhancement on MRI examination were the most significant parameters influencing OS. Specifically, GCB cases exhibited a better prognosis, with a longer OS (16 months), while Non-GCB cases had a worse prognosis with a shorter OS (8 months). Further, cases with higher MRI enhancement values, corresponding to the GCB subtype, had longer survival than cases with lower enhancement values, which aligned with the Non-GCB subtype. Therefore, more adequate treatment adjustments should be based on imaging too, suggesting different strategies regarding immune checkpoint inhibitors and chimeric antigen receptor (CAR) T cells; thus, immediate therapeutic applicability should be hypothesized for more aggressive Non-GCB cases.

Finally, the association of morphological and neuroradiological characteristics in PCNSL-DLBCL may provide a significant prognostic tool to better define patients' OS, advocating for a multidisciplinary approach in brain lymphoid neoplasms. This desirable setting may prevent conflicting data reported in the literature that exclusively refer to morphological parameters such as immunophenotype and Ki67 value (15,27). In conclusion, we assert that PCNSL is characterized by specific clinicopathological and neuroradiological features (older age, supratentorial site, Non-GCB immunoprofile, and MRI enhancement); however, the limited sample size of the present cohort may introduce bias into the investigation, necessitating further multicentric studies to corroborate our results. Although the small cohort analyzed and the single-center retrospective nature of the study may influence statistics, introducing selection bias and limiting generalizability, particularly for some subgroups (e.g., age/sex), the reduced interpretability of data may arise from non-significant ADC-Ki67 correlation, rendering potential confounders less prominent (e.g., tumor microenvironment heterogeneity, cellular density).

Acknowledgements

Not applicable.

Funding

No funding was received.

Availability of data and materials

The data generated in the present study may be requested from the corresponding author.

Authors' contributions

IR, CP, FG, AI and GT developed the study design and drafted the manuscript. IR, CP, SCS, VF, MM and AG were involved in data acquisition and interpretation. AI, FG and GT reviewed the manuscript. AG, FG and GT confirm the authenticity of all the raw data. All authors have read and approved the final version of the manuscript.

Ethical approval and consent to participate

The analysis was conducted according to the Good Clinical Practice guidelines and the Declaration of Helsinki (1975,

revised in 2013). Before surgical procedures, all patients provided written, anonymized and informed consent. Pathology reports and medical records were thoroughly reviewed. Patient initials and other personal identifiers were removed from all images. The Institutional Review Board of the University Hospital of Messina (Messina, Italy) approved the present study (approval no. N. 47/19; May 2, 2019).

Patient consent for publication

Written informed consent was obtained from all patients for the publication of their data.

Competing interests

The authors declare that they have no competing interests.

References

1. Liu Y, Yao Q and Zhang F: Diagnosis, prognosis and treatment of primary central nervous system lymphoma in the elderly population (Review). Int J Oncol 58: 371-387, 2021.
2. Shao L, Xu C, Wu H, Jamal M, Pan S, Li S, Chen F, Yu D, Liu K and Wei Y: Recent progress on primary central nervous system lymphoma-From bench to bedside. Front Oncol 11: 689843, 2021.
3. Ferreri AJM, Calimeri T, Cwynarski K, Dietrich J, Grommes C, Hoang-Xuan K, Hu LS, Illerhaus G, Nayak L, Ponzoni M and Batchelor TT: Primary central nervous system lymphoma. Nat Rev Dis Primers 9: 29, 2023.
4. D'Angelo CR: Diagnostic, pathologic, and therapeutic considerations for primary CNS lymphoma. JCO Oncol Pract 20: 195-202, 2024.
5. Green K, Munakomi S and Hogg JP: Central nervous system lymphoma. In: StatPearls [Internet]. Treasure Island (FL), StatPearls Publishing, 2024.
6. Schaff LR and Grommes C: Primary central nervous system lymphoma. Blood 140: 971-979, 2022.
7. de Koning ME, Hof JJ, Jansen C, Doorduijn JK, Bromberg JEC and van der Meulen M: Primary central nervous system lymphoma. J Neurol 271: 2906-2913, 2024.
8. Lebrun L, Allard-Demoustiez S and Salmon I: Pathology and new insights in central nervous system lymphomas. Curr Opin Oncol 35: 347-356, 2023.
9. Jin Q, Jiang H, Han Y, Zhang L, Li C, Zhang Y, Chai Y, Zeng P, Yue L and Wu C: Tumor microenvironment in primary central nervous system lymphoma (PCNSL). Cancer Biol Ther 25: 2425131, 2024.
10. Bödör C, Alpár D, Marosvári D, Galik B, Rajnai H, Bátai B, Nagy Á, Kajtár B, Burján A, Deák B, *et al*: Molecular subtypes and genomic profile of primary central nervous system lymphoma. J Neuropathol Exp Neurol 79: 176-183, 2020.
11. Hans CP: Confirmation of the molecular classification of diffuse large B-cell lymphoma by immunohistochemistry using a tissue microarray. Blood 103: 275-282, 2004.
12. Joshi A, Deshpande S and Bayaskar M: Primary CNS lymphoma in immunocompetent patients: Appearances on conventional and advanced imaging with review of literature. J Radiol Case Rep 16: 1-17, 2022.
13. Radotra BD, Parkhi M, Chatterjee D, Yadav BS, Ballari NR, Prakash G and Gupta SK: Clinicopathological features of primary central nervous system diffuse large B cell lymphoma: Experience from a tertiary center in North India. Surg Neurol Int 11: 424, 2020.
14. Ribas GA, de Mori LH, Freddi TAL, Oliveira LDS, de Souza SR and Corrêa DG: Primary central nervous system lymphoma: Imaging features and differential diagnosis. Neuroradiol J 37: 705-722, 2024.
15. Liu J, Wang Y, Liu Y, Liu Z, Cui Q, Ji N, Sun S, Wang B, Wang Y, Sun X and Liu Y: Immunohistochemical profile and prognostic significance in primary central nervous system lymphoma: Analysis of 89 cases. Oncol Lett 14: 5505-5512, 2017.
16. Puligundla CK, Bala S, Karnam AK, Gundeti S, Paul TR, Uppin MS and Maddali LS: Clinicopathological features and outcomes in primary central nervous system lymphoma: A 10-year experience. Indian J Med Paediatric Oncol 38: 478-482, 2017.
17. Du KX, Shen HR, Pan BH, Luthuli S, Wang L, Liang JH, Li Y, Yin H, Li JY, Wu JZ and Xu W: Prognostic value of POD18 combined with improved IELSG in primary central nervous system lymphoma. Clin Transl Oncol 26: 720-731, 2023.
18. Yokogami K, Azuma M, Takeshima H and Hirai T: Lymphomas of the central nervous system. Adv Exp Med Biol 1405: 527-543, 2023.
19. Provenzale JM, Mukundan S and Dewhirst M: The role of blood-brain barrier permeability in brain tumor imaging and therapeutics. AJR Am J Roentgenol 185: 763-767, 2005.
20. White NS, McDonald CR, Farid N, Kuperman JM, Kesari S and Dale AM: Improved conspicuity and delineation of high-grade primary and metastatic brain tumors using 'restriction spectrum imaging': Quantitative comparison with high B-value DWI and ADC. AJNR Am J Neuroradiol 34: 958-964, 2013.
21. Ahn SJ, Shin HJ, Chang JH and Lee SK: Differentiation between primary cerebral lymphoma and glioblastoma using the apparent diffusion coefficient: Comparison of three different ROI methods. PLoS One 9: e112948, 2014.
22. Chen J, Xia J, Zhou YC, Xia LM, Zhu WZ, Zou ML, Feng DY and Wang CY: Correlation between magnetic resonance diffusion-weighted imaging and cell density in astrocytoma. Zhonghua Zhong Liu Za Zhi 27: 309-311, 2005 (In Chinese).
23. Guo AC, Cummings TJ, Dash RC and Provenzale JM: Lymphomas and high-grade astrocytomas: Comparison of water diffusibility and histologic characteristics. Radiology 224: 177-183, 2002.
24. Schob S, Meyer J, Gawlitza M, Frydrychowicz C, Müller W, Preuss M, Bure L, Quäschling U, Hoffmann KT and Surov A: Diffusion-weighted MRI reflects proliferative activity in primary CNS lymphoma. PLoS One 11: e0161386, 2016.
25. Surov A, Meyer HJ and Wienke A: Correlation between apparent diffusion coefficient (ADC) and cellularity is different in several tumors: A meta-analysis. Oncotarget 8: 59492-59499, 2017.
26. Morales-Martinez A, Nichelli L, Hernandez-Verdin I, Houillier C, Alentorn A and Hoang-Xuan K: Prognostic factors in primary central nervous system lymphoma. Curr Opin Oncol 34: 676-684, 2022.
27. Momota H, Narita Y, Maeshima AM, Miyakita Y, Shinomiya A, Maruyama T, Muragaki Y and Shibui S: Prognostic value of immunohistochemical profile and response to high-dose methotrexate therapy in primary CNS lymphoma. J Neurooncol 98: 341-348, 2010.